Clinical and Experimental Medicine (2025) 25:154
https://doi.org/10.1007/s10238-025-01696-x

RESEARCH

Revealing roles of PANoptosis-related genes in prognosis and molecular subtypes in lung squamous cell carcinoma by integrated bioinformatic analyses and experiments

Ying Chen[1] · Meihua Wang[1]

Received: 19 February 2025 / Accepted: 14 April 2025

Abstract

The purpose of current study was to reveal the role of PANoptosis-associated genes in lung squamous cell carcinoma (LUSC) and their potential as prognostic biomarkers. We analyzed RNA-seq data from TCGA-LUSC and GEO datasets to identify differentially expressed genes (DEGs) between LUSC and normal samples, followed by VENN analysis to reveal PANoptosis-related DEGs. Functional enrichment analyses were performed by clusterProfiler package. Distinct LUSC subtypes were identified by consensus clustering based on PANoptosis-related DEGs. Univariate Cox and LASSO regression were utilized to identify key prognostic genes, and a prognostic model was developed based on selected genes. Immune infiltration status was evaluated by CIBERSORT and ESTIMATE algorithms. Expression of key prognostic genes was tested in three LUSC cell lines by RT-qPCR and Western blot. Roles of TLR3 in LUSC progression were determined by functional experiments. A total of 76 PANoptosis-related DEGs were identified, with significant enrichment in apoptosis pathways. The clustering analysis revealed four subtypes, in which survival and immune microenvironment were dramatically different. From the 76 genes, four key prognostic genes (CHEK2, PDK4, TLR3, and IL1B) were identified to establish prognostic risk model, which could reflect the survival status and immune cells composition variations for LUSC patients. Besides, these four genes showed significant correlations with infiltrating levels of various immune cells. TLR3 was identified as a more weighted prognostic risk gene in LUSC. Functional assays demonstrated that genes like TLR3 modulated cell proliferation, migration, and inflammatory responses in LUSC cells. This study highlighted the potential of the four key PANoptosis genes as biomarkers or targets in LUSC, and the risk model based on these four genes provided novel insights to develop personalized treatment strategy for patients with LUSC.

✉ Meihua Wang
2546711274@qq.com

[1] Department of Respiratory Medicine, Hangzhou Xixi Hospital Affiliated to Zhejiang Chinese Medical University (Hangzhou Xixi Hospital), No. 2 Hengbu Road, Hangzhou 310023, Zhejiang, China

Published online: 12 May 2025

Graphical Abstract

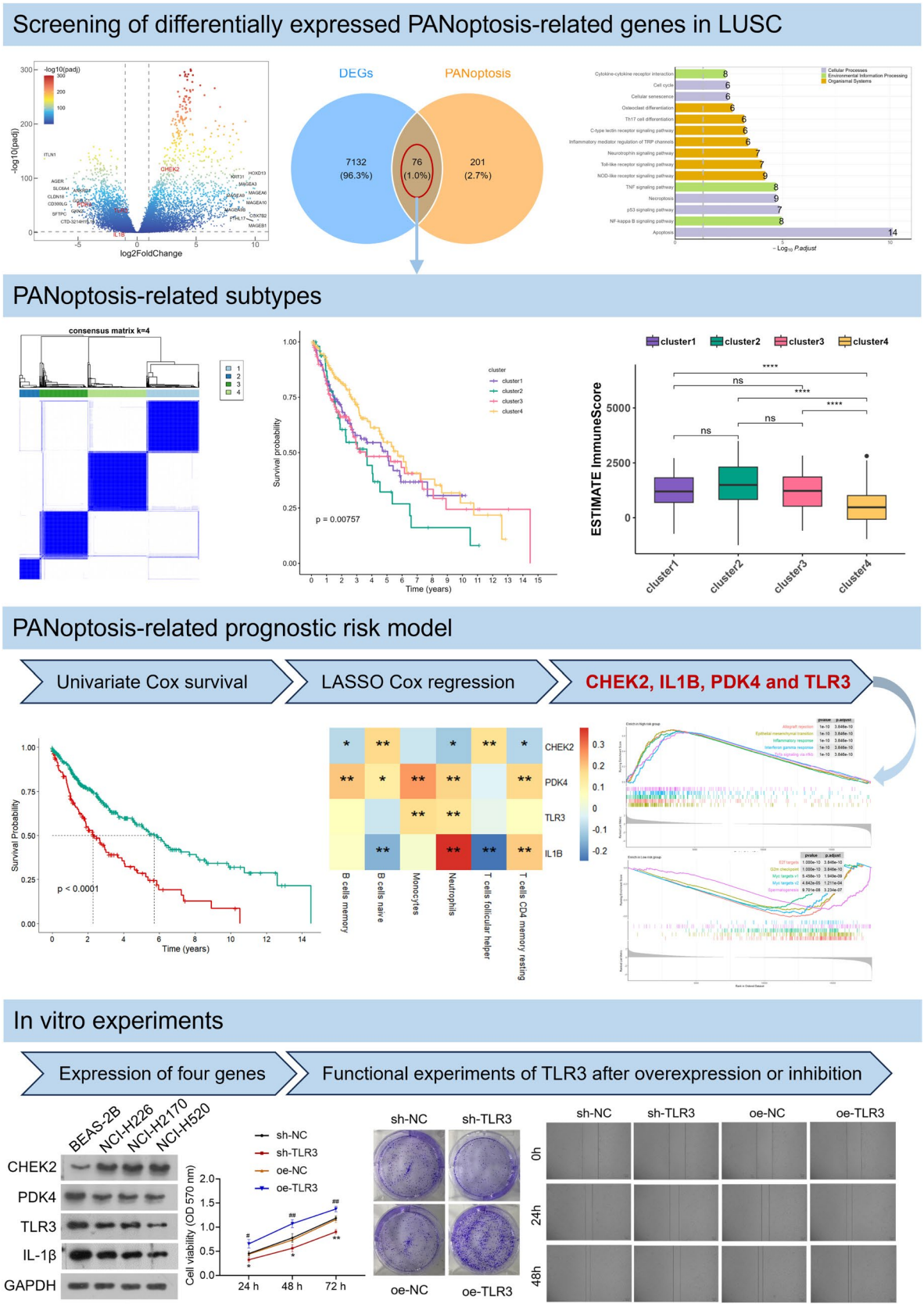

Keywords LUSC · PANoptosis-associated genes · Prognostic model · Immune microenvironment · Enrichment analysis · Validation analysis

Introduction

Lung squamous cell carcinoma (LUSC), one of the primary forms of lung cancer, has a high degree of malignancy and poor prognosis [1]. Patients with advanced LUSC exhibited approximately 30% shorter of median survival after first-line treatment than those other non-small cell lung cancer (NSCLC) subtypes in comparative clinical studies [2, 3]. Despite the advancements in targeted therapies and immunotherapies for LUSC, the overall survival rate for patients with this condition remains suboptimal due to genetic heterogeneity and the complexity of the tumor microenvironment [4]. Meanwhile, some LUSC patients lack targetable cancer-causing mutations or develop resistance to existing treatments [5, 6]. Such situations lead to the main task for developing new ways to distinguish LUSC patients who might benefit from aggressive treatments. Hence, there is a need to search for new biomarkers to provide information about prognosis or therapy responses for LUSC.

PANoptosis is a recently proposed mode of programmed cell death that integrates characteristic with apoptosis, pyroptosis, and necroptosis, representing a common pathway for these cellular death processes [7], which can mediate a broad response to both intrinsic and extrinsic stress signals by simultaneously activating multiple cell death pathways [8]. Therefore, PANoptosis plays a critical regulatory role in various pathophysiological processes, including antiviral immunity, tumorigenesis, and inflammatory responses [9]. Recent studies have increasingly indicated that differentially expression of PANoptosis contribute to the progression of various tumors, particularly in malignancies intertwined with complex immune microenvironments, such as in lung cancer [10]. Zhang et al. identified six PANoptosis-associated differentially expressed genes (DEGs) such as NLRC4 and MLKL in lung adenocarcinoma (LUAD), and these six genes exhibited closely associations with prognosis, tumor stemness and therapy response [11]. Several recent studies also investigated the roles of PANoptosis-related genes in molecular subtypes classification and in predicting prognosis, tumor immunity and therapy effect in LUAD [12–14]. Unlike the intensive investigations in LUAD, there has no study to explore the exact roles of PANoptosis-related genes in LUSC. Therefore, we conducted this study to fill this research gap.

In this study, roles of PANoptosis-related genes in LUSC were comprehensively explored by integrated bioinformatic analyses and in vitro experiments. First, based on the PANoptosis-related DEGs in LUSC, consensus clustering was conducted to investigate the molecular subtypes of LUSC that differed in survival and tumor microenvironment (TME). Second, the prognostic value of PANoptosis-related DEGs was explored, and a prognostic model was established for predicting prognosis of patients with LUSC. Besides, correlations of this prognostic signature with immune infiltration and drug sensitivity as well as activity of signaling pathways were illustrated. Third, the expression of these PANoptosis-related genes in LUSC cell lines was validated through cellular experiments, and their functions and mechanisms in LUSC were further investigated. Through this integrated approach, we hoped to reveal the function of PANoptosis in LUSC and to discover new molecular targets for future personalized treatments of this disease.

Materials and methods

Dataset and pre-processing

A TCGA-LUSC dataset (496 LUSC samples and 49 normal samples), as well as associated survival information, was provided by the UCSC Xena database [15]. Meanwhile, the dataset GSE73403 and associated survival information in Gene Expression Omnibus (GEO) database [16] were enrolled in this investigation. GSE73403 contained 69 samples from LUSC patients. The data were generated on the platform of GPL6480 Agilent-014850. Using the probe expression matrix and the annotation file, we excluded probes that did not match any gene symbols. When multiple probes were linked to a single gene, the average expression value of those probes was calculated for that gene. Furthermore, we identified 277 genes associated with PANoptosis from a previously published study by Song et al. [17].

PANoptosis-related DEGs investigation

DEGs between LUSC and normal samples from TCGA-LUSC were analyzed using the DESeq2 package in R [18]. In summary, the significance of gene expression was assessed based on log2 fold change (FC) > 1 and P value < 0.05. The results were then visualized with a volcano plot. Then, a VENN plot analysis was performed based on DEGs and PANoptosis-associated genes to explore the PANoptosis-related DEGs by using ggvenn package in R (version: 0.1.10).

Functional enrichment and protein–protein interaction (PPI) network analysis

GO function and KEGG pathway analyses were conducted on PANoptosis-related DEGs using clusterProfiler package

of R [19] with the cutoff value of P value < 0.05. Then, according to STING database (version: 11.0) [20], the protein interaction information was extracted, and PPI pairs (median confidence = 0.4) among PANoptosis-related DEGs were predicted. Finally, the Cytoscape (version: 3.7.1) software [21] was applied to visualize the current network.

Clustering analysis for PANoptosis-related DEGs

To investigate different clusters of LUSC associated with PANoptosis, the ConsensusClusterPlus package [22] in R software was used for analysis based on TCGA-LUSC dataset. Kaplan–Meier (KM) survival analysis was carried out on clusters based on the Survival package (version 2.41-1). Subsequently, the ESTIMATE algorithm [23] was then utilized to investigate the stromal scores, immune scores, ESTIMATE scores, and tumor purity across various clusters. A P value below 0.05 was deemed statistically significant. The findings were represented using a box plot.

Prognostic model construction and validation

The univariate Cox regression investigation was applied on PANoptosis-related DEGs to reveal prognostic genes with $P < 0.05$. Using LASSO Cox regression in R [24], the optimal gene set was identified from prognostic genes in the TCGA-LUSC training dataset through tenfold cross-validation with the glmnet package. Then, based on the prognostic coefficient of key genes obtained above, a risk model was developed, followed by the risk score (RS) calculated. Subsequently, patients were divided into high-risk group and low-risk group based on the optimal cutoff value obtained by surv_cutpoint method in survival package (version: 3.5–8) of R. In addition, KM curve was utilized to assess survival outcomes in two risk groups. The predictive performance of the prognostic model was evaluated by generating a ROC curve. In addition, a further validation analysis on model was also performed based on GSE73403. Finally, the GSEA enrichment scores for each pathway in both groups were calculated and ranked using the Benjamini–Hochberg (BH) method with $P < 0.05$, utilizing the clusterProfiler package in R. The top five pathways for each enrichment result were identified based on the normalized enrichment score (NES).

Immune infiltration analysis

The CIBERSORT methodology [25] was applied to investigate the infiltration levels of 22 types of immune cells within the tumor samples. To unveil differences in immune cell compositions in different risk group, the ESTIMATE analysis was employed [26]. Moreover, the link between key genes obtained above and different immune cells, as well as among different cell types, was assessed using the Pearson correlation coefficient [27]. The results were visualized using heat map. Furthermore, the expression levels of key immune checkpoint genes, such as CD274, CTLA4, HAVCR2, LAG3, PDCD1, and LMTK3, were obtained, and the differences in expression between different risk groups were evaluated through an t test.

Drug sensitivity analysis

The oncoPredict package in R was applied to explore the sensitivity of various drugs [28]. The difference of sensitivity (IC50 value) for chemotherapy drugs was quantified by using the calcPhenotype algorithm in TCGA-LUSC dataset. Significant differences in drug sensitivity between different risk groups were assessed using the t test. The result was visualized using box plot.

Cell culture

BEAS-2B (SUNNCELL, SNL-203), a human lung epithelial cell line, as well as three LUSC cell line including NCI-H2170 (Pricella, CL-0394), NCI-H520 (Pricella, CL-0402) and NCI-H226 (Pricella, CL-0396), was kept in RPMI-1640 medium (Pricella, PM150110), which further mixed with 10% fetal bovine serum, 100 U/mL penicillin, and 100 µg/mL streptomycin until they reached 90% confluence (at 37 °C and 5% CO_2). All cells were cultured consistently between the second and third generations, and culture supernatant and cell samples were harvested for analysis after 24 h.

Lentiviral vectors construction and transfection

The sh-TLR3 (SS: GAGTTGTCATCGAATCAAA; AS: TTTGATTCGATGACAACTC), which designed based on Designer of Small Interfering RNA website, was introduced into lentiviral plasmid vectors. In addition, oe-TLR3 was designed by NCBI website. In summary, lentiviral shuttle plasmids and their associated packaging plasmids were generated, and high-purity, endotoxin-free plasmids were isolated using a reagent kit (Tiangen Biochemical Technology Co., Ltd., Beijing). These plasmids were then co-transfected into cells, while an empty lentiviral vector served as the negative control. After 18 h of transfection, the medium was replaced with complete culture medium. Following an additional 24-h incubation, the supernatant rich in lentiviral particles was collected and concentrated through ultracentrifugation. The viral titer was assessed using a fluorescence counting method, and the packaged virus was utilized for subsequent experiments. For lentiviral infections, NCI-H226 cells were kept in a 6-well plate, and lentivirus ($1 \times 10\hat{}8$ TU/mL) was added to the medium when the cells

reached 70–90% confluence. Following 48 h for infections, 2 μg/mL puromycin was added to stable transfected cells.

qRT-PCR

To explore the mRNA expression of signature genes (CHEK2, PDK4, TLR3 and IL1β) identified in this study, the qRT-PCR assay was conducted based on each cell lines. Total RNA was extracted from the cells with TRIZOL reagent (Invitrogen, 15,596,018), and cDNA was synthesized using the 5 × FastKing-RT SuperMix (TsingKe, KR118-02). PCR analysis was achieved by a RT-qPCR instrument (Bio-Rad, CFX96Touch) with an initial denaturation step at 95 °C for 10 min, followed by 40 cycles of denaturation at 95 °C for 12 s and annealing/extension at 60 °C for 40 s. Relative expression levels were determined using the $2^{-\Delta\Delta Ct}$ method [29]. Primer details are provided in Supplementary Table 1.

Western blotting

The western blotting assay in current study was used to evaluate the expression of CHEK2, PDK4, TLR3 and IL1β. Briefly, total protein was obtained based on cells in each group with the help of RIPA lysate (Beyotime, P0013B). Bicinchoninic acid (BCA) protein quantitative kit Solarbio (PC0020) was used in current study for the quantitative investigation. Following denaturation, the proteins were isolated with the help of 10% SDS-PAGE electrophoresis (Beyotime, ST628) and subsequently moved to a polyvinylidene fluoride (PVDF) membrane (Beyotime, FFP24). At ambient temperature, the cellular membrane was sealed with a TBS solution containing 5% BSA for 1 h. before adding primary antibody including Anti-CHEK2 antibody (Abclonal rabbit monoclonal, 1:2000, A19543), Anti-p-IL1β antibody (Abclonal rabbit monoclonal, 1:1000, A22257), Anti-TLR3 antibody (Abcam Rabbit polyclonal, 2 g/mL, ab62566), Anti-PDK4 antibody (Abclonal Rabbit polyclonal, 1:1000, A13337) and Anti-GAPDH antibody (Affinity Rabbit polyclonal, 1:3000, AF7021) used at manufacturer-recommended dilutions. Subsequently, sections were mixed with the Affinity goat anti-rabbit IgG H&L (HRP) secondary antibody (1:2000, ab205718) for 60 min at room temperature. Protein bands were then developed using ECL reagents, followed by images capturing.

MTT assay

The proliferative ability of cells was investigated by MTT. Simply, according to the instruction of MTT cell proliferation and cytotoxicity detection kit (Beyotime, C0009S), a total of 10 μl MTT (5 mg/mL) was seeded in each well. After 4 h of culturing, the medium was removed, and 100 μl Formazan solution was added into each well. Optical density (OD) at 570 nm was detected by a detector (Biotek, Synergy HTX).

Wounding healing assay to detect cell migration

Wounding healing assay was carried out to elucidate the cell migration. All cells were seeded onto 6-well dishes (5×10^5 cell/well) and wounded using a marker pen. Detached cells were eliminated by PBS washing on samples, followed by incubated in an incubator (37 °C, 5% CO_2). The plates were photographed at 0 h, 24 h and 48 h, respectively.

Colony formation assay

Following lentivirus treatment, stably transfected cells were trypsinized, counted, and seeded into a 6-well plate at a density of 200 cells per well. Cells allowed to grow for 7 days to form colonies. Afterward, the colonies were stained with crystal violet (Beyotime, C0121) for 20 min. The stained colonies were imaged with a fluorescence microscope, and the overall number of colonies (50 cells each) was quantified and examined.

Enzyme-linked immunosorbent assay (ELISA)

ELISA kits were applied to explore the expression levels of immune factors including IL1β (Beyotime, PI305), TNF-α (Mlbio, ml064303), IFN-γ (Mlbio, ml057856) and VEGF (Mlbio, ml064255) in supernatant.

Statistical analysis

R software (version 4.3.3) in this study was used as tool for statistical analysis. The comparison of differences between the two groups in current study was carried out with the help of Wilcoxon rank test. In addition, the relationship between groups was carried out in our study with the help of Spearman correlation analysis. A two-sided P value of < 0.05 was considered statistically significant.

Results

PANoptosis-related DEGs investigation

Totally, 7208 DEGs were screened in LUSC vs. controls, of which 4222 genes were upregulated, while 2986 genes were downregulated in LUSC than in controls (Fig. 1A). Then, based on the intersection of DEGs with the PANoptosis-related genes, the VENN plot analysis showed totally 76 common genes, and these genes were

regarded as PANoptosis-related DEGs (Fig. 1B). These genes were predominantly enriched in cell death-related KEGG pathways such as apoptosis, necroptosis, and in immune-inflammatory-related pathways, such as Th17 cell differentiation, inflammatory mediator regulation of TRP channels, TNF signaling pathway and Toll-like receptor signaling pathway (Fig. 1C). Meanwhile, these genes were primarily assembled in 707 functions like intrinsic apoptotic signaling (GO: 0097193), extrinsic apoptotic signaling pathway (GO: 0097191) and anoikis (GO: 0043276) (Fig. 1D). In addition, with median confidence = 0.4, a PPI network was constructed with these PANoptosis-related DEGs, in which these genes interacted with each other closely (Fig. 1E). This suggested that these genes might function as functional complexes.

PANoptosis-related molecular clusters

A total of four clusters of LUSC associated with PANoptosis-related DEGs (Fig. 2A) were identified as the optimal clustering. The heatmap analysis confirmed the result of clustering (Fig. 2B). Then, the clusters' distribution was confirmed by the t-SNE plot (Fig. 2C). The KM analysis proved that the survival of patients with LUSC could be separated by different clusters (Fig. 2D). Compared with other three clusters, the cluster 4 had a higher survival probability based on survival analysis. In addition, the cluster 2 had the bad survival probability when compared with other three clusters. Moreover, the tumor microenvironment analysis of clusters showed that tumor purity in the cluster 4 was dramatically higher compared to that in Cluster 1, 2 and 3 (all $P < 0.05$). Conversely, cluster 1, 2 and 3 exhibited significantly higher stromal and immune cell scores, reflecting a high overall immune infiltration in their microenvironment compared to cluster 4 (Fig. 2E–H).

PANoptosis-related prognostic risk model

Based on the 76 PANoptosis-related DEGs that significantly related to LUSC, combined with their expression values and survival status, totally 4 prognostic genes were selected by using univariate Cox expression algorithm (Fig. 3A). These

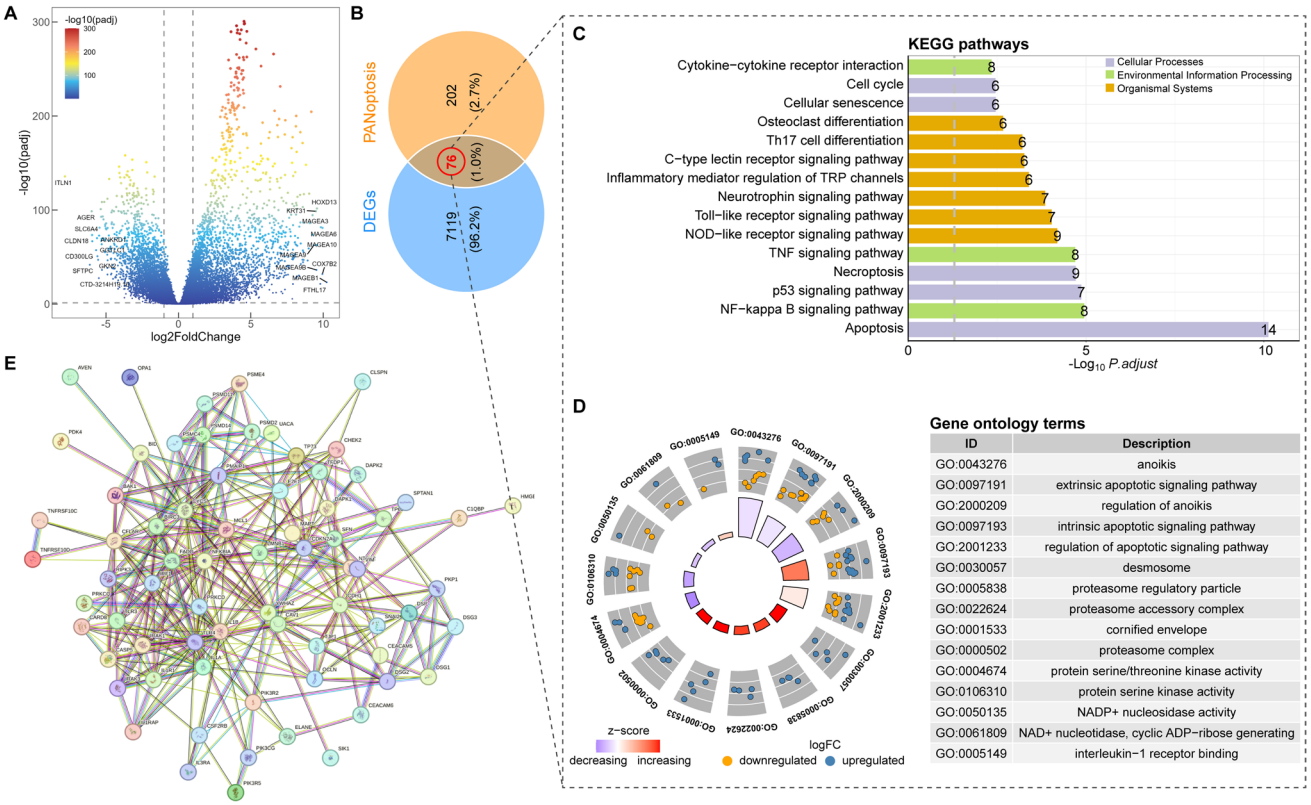

Fig. 1 The PANoptosis-associated differentially expressed genes (PANoptosis-related DEGs) investigation in current study. **A**, the volcano plot showed the differentially expressed genes (DEGs) between lung squamous cell carcinoma (LUSC) samples and normal samples. B, totally 76 PANoptosis-related DEGs revealed by the VENN plot analysis. C, the bar-chart showed the significant KEGG pathways enriched by PANoptosis-related DEGs in current analysis. D, the significant GO functions assembled by PANoptosis-related DEGs in current analysis. E, the protein–protein interaction (PPI) network constructed by PANoptosis-related DEGs: The nodes represented the PANoptosis-related DEGs, while the line between two nodes represented interaction

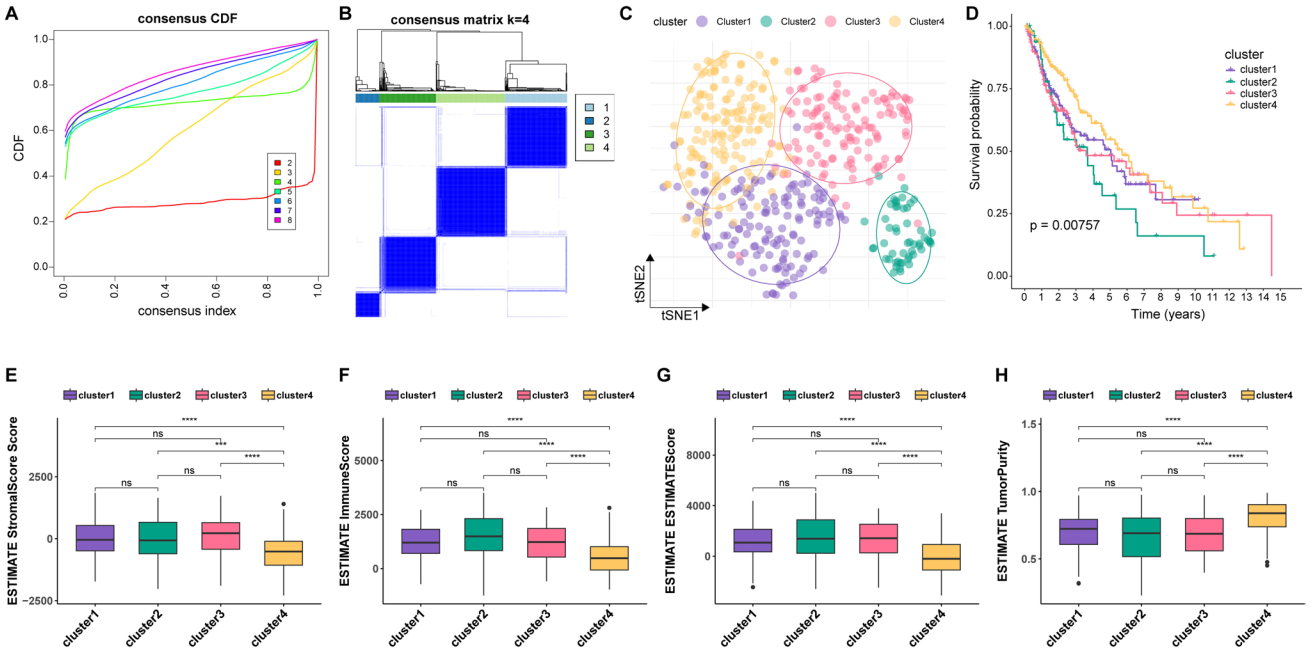

Fig. 2 The clustering analysis of PANoptosis-related DEGs-associated LUSC. **A**, the clustering analysis based on PANoptosis-related DEGs-associated LUSC by using consistency clustering empirical cumulative distribution function (CDF). B, the heatmap of consistency clustering analysis revealed four clusters. C, the results of t-distributed stochastic neighbor embedding (t-SNE) analysis for clusters distributed. D, the Kaplan–Meier (KM) analysis for clinical survival prognosis of clusters. E–H, the box plot analysis showed that expression of four clusters based on stromal score, immune score, estimate score and tumor purity, respectively. ***, $P<0.001$; ****, $P<0.0001$

four genes were further analyzed by LASSO regression, and all the four genes were determined (Fig. 3B). Using Lasso regression coefficient of these four optimal genes including CHEK2, PDK4, TLR3 and IL1B, a prognostic model was constructed (Formula: Risk = CHEK2 × − 0.306 + PDK4 × 0.056 + TLR3 × 0.0762 + IL1B × 0.0697). Then, samples were assigned into two different risk groups. The expression of four model genes as well as different clinical characteristic between two risk groups is showed in Fig. 3C. The result indicated that expression of CHEK2 was decreased gradually with the increase in risk score, while expression of other three genes showed opposite trends with CHEK2. The KM analysis of the training data indicated that the survival rate in the high-risk group was significantly lower compared to the low-risk group ($P<0.0001$) (Fig. 3D). The AUC value in ROC curve in training data was larger than 0.614, indicated a moderate prognostic value of current model in training data (Fig. 3D). Risk curve analysis of the training dataset showed lower mortality outcomes in the low-risk group compared to the high-risk group based on follow-up data, further highlighting clinical value of our model (Fig. 3E). Moreover, the analysis results based on validation dataset confirmed the prognostic value of this model via KM survival (Fig. 3F), ROC curve (Fig. 3F) and risk curve analysis (Fig. 3G). In addition, with $P<0.05$, a total of 20 KEGG pathways that significantly activated in high-risk group, as well as 9 pathways in low-risk group, were revealed by GSEA. The TOP 5 results of enrichment analysis for different risk groups are showed in Fig. 3H. The result indicated that pathways such as epithelial mesenchymal transition, inflammatory response, interferon gamma response and TNF-α signaling via NFκB were significantly activated in high-risk group. Meanwhile, E2F targets, G2M checkpoint and Myc targets were dramatically enriched in low-risk group. To further explore the connection between molecular clusters and risk groups, we added a Sankey diagram. As shown in Fig. 3I, majority of the patients in cluster 4 were assigned into low-risk group, and patients in low-risk group tended to be alive. As for patients in cluster 1–3, over half of these patients were assigned into high-risk group. These findings were consistent with the prognosis analysis in molecular clusters.

Immune infiltration and drug sensitive analysis

The fraction of 22 cells associated with immune in TCGA dataset was estimated by using CIBERSORT algorithm. With $P<0.05$, totally six immune cells, including memory B cells, naive B cells, monocytes, neutrophils, resting memory CD4 + T cells and follicular helper T cells, were revealed dramatically different expressed between two risk groups (Fig. 4A). For instance, neutrophil levels were markedly reduced in the low-risk group compared to the high-risk

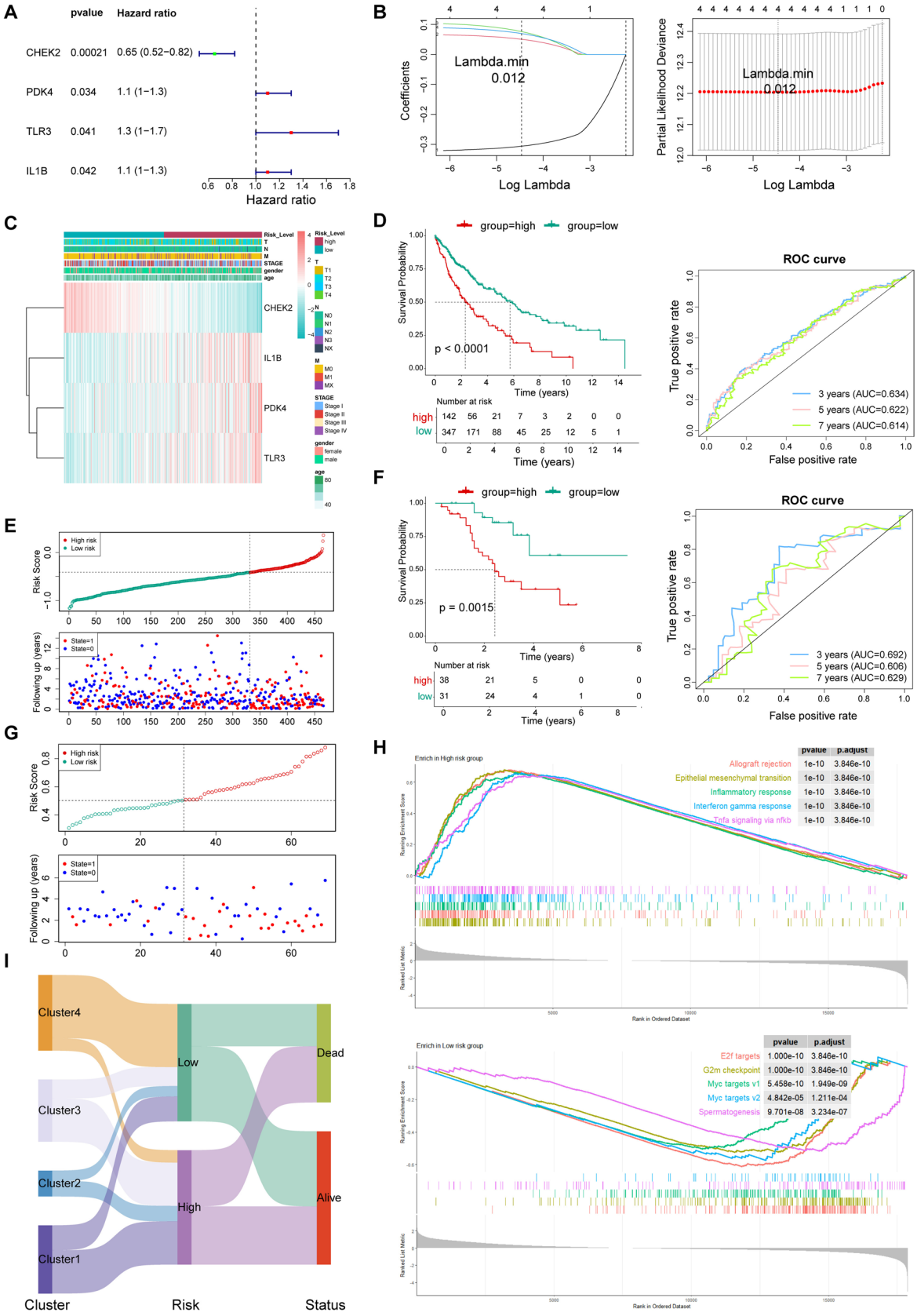
A
pvalue
Hazard ratio
CHEK2 0.00021 0.65 (0.52−0.82)
PDK4 0.034 1.1 (1−1.3)
TLR3 0.041 1.3 (1−1.7)
IL1B 0.042 1.1 (1−1.3)
Hazard ratio
B
Lambda.min
0.012
Coefficients
Log Lambda
Partial Likelihood Deviance
C
CHEK2
IL1B
PDK4
TLR3
D
group=high
group=low
p < 0.0001
Survival Probability
Time (years)
Number at risk
high 142 56 21 7 3 2 0 0
low 347 171 88 45 25 12 5 1
ROC curve
True positive rate
False positive rate
3 years (AUC=0.634)
5 years (AUC=0.622)
7 years (AUC=0.614)
E
High risk
Low risk
Risk Score
State=1
State=0
Following up (years)
F
p = 0.0015
high 38 21 5 0 0
low 31 24 4 1 0
3 years (AUC=0.692)
5 years (AUC=0.606)
7 years (AUC=0.629)
G
H
Enrich in High risk group
Allograft rejection 1e-10 3.846e-10
Epithelial mesenchymal transition 1e-10 3.846e-10
Inflammatory response 1e-10 3.846e-10
Interferon gamma response 1e-10 3.846e-10
Tnfa signaling via nfkb 1e-10 3.846e-10
Enrich in Low risk group
E2f targets 1.000e-10 3.846e-10
G2m checkpoint 1.000e-10 3.846e-10
Myc targets v1 5.458e-10 1.949e-09
Myc targets v2 4.842e-05 1.211e-04
Spermatogenesis 9.701e-08 3.234e-07
I
Cluster4
Cluster3
Cluster2
Cluster1
Low
High
Dead
Alive
Cluster
Risk
Status

◂**Fig. 3** The prognostic model construction and validation. **A**, the result of univariate Cox expression. **B**, the variation of LASSO regression coefficients with the regularization parameter Lambda, as well as the model performance curve based on cross-validation. **C**, the heatmap of clinical features and prognostic genes in the training set. **D**, the result of KM survival analysis for current prognostic model constructed with 4 genes in training data: The red line represented the high-risk group of GBM, while the green line represented the low-risk group of LUSC; the X-axis represented the survival time, while the Y-axis represented the survival probability; $P < 0.05$ was considered as significant different. The ROC analysis in training data revealed the AUC value of 3-, 5- and 7-year survival: The different color represented different survival time; the X-axis represented specificity, while the Y-axis represented the sensitivity. **E**, the risk curve analysis based on training dataset. **F**, the result of KM survival analysis for current prognostic model constructed with 4 genes in validation data. The ROC analysis in validation data revealed the AUC value of 3-, 5- and 7-year survival. **G**, the risk curve analysis based on validation dataset. **H**, the TOP 5 results of significantly enriched KEGG pathways in high-risk group and low-risk group. **I**, the Sankey diagram showing the connections among molecular clusters, risk groups and survival status of patients

group ($P < 0.001$). In contrast, follicular helper T cell levels were considerably elevated in low-risk group compared to high-risk group ($P < 0.001$). The correlation analysis for 22 cells and 4 prognostic genes is displayed in Fig. 4B. For example, TLR3 was significantly correlated with both neutrophils and monocytes (all $P < 0.05$). The abundance of neutrophil infiltration was significantly corresponded with all four prognostic genes' expression (all $P < 0.05$). In addition, analysis of six immune checkpoint expressions between the two risk groups revealed that LAG3, CTLA4, HAVCR2, and PDCD1 levels were all significantly elevated in the high-risk group compared to the low-risk group (all $P < 0.05$) (Fig. 4E). However, the expression difference of LMTK3 and CD274 between two risk groups was not significant. Furthermore, the sensitive analysis between two risk groups was performed based on 198 anti-tumor drugs. According to the TOP 20 results, patients in the high-risk group exhibited increased sensitivity to drugs like AZD5582, AZD8186, Nutlin-3a, PD0325901 (Mirdametinib), PRIMA-1MET (Prima-1) and PRT062607, Topotecan (Fig. 4D).

Validation of key prognostic genes in human LUSC cells

To validate the identified key genes' expression (CHEK2, PDK4, TLR3, and IL1β) in human LUSC cell lines and normal lung epithelial cells, qRT-PCR and Western blot assays were performed (Fig. 5). In comparison with the normal BEAS-2B cells, CHEK2 mRNA (Fig. 5A) and protein levels (Fig. 5B) were significantly upregulated in the LUSC cell lines NCI-H226, NCI-H2170, and NCI-H520 (all $P < 0.01$). In contrast, when compared to BEAS-2B cells, PDK4, TLR4 and IL1β exhibited a notable downregulation in these cancer cell lines, both at the mRNA (Fig. 5A) and protein levels (Fig. 5B). Particularly, TLR3 expression demonstrated a distinctive lower expression in the NCI-H520 cells than in the NCI-H226 and NCI-H2170 cells. The differential expression pattern of these four genes between normal lung epithelial cells and LUSC cells was consistent with findings from above analyses, suggesting their potential role in the pathogenesis of LUSC.

TLR3 modulated cell proliferation, migration and inflammatory response in LUSC

Among the four prognostic genes, TLR3 was identified as risk factor in LUSC and had a highest hazard ratio than others. Therefore, TLR3 was selected for further investigation. To explore the role of TLR3 in LUSC, lentiviral transfection was employed to knock down (sh-TLR3) or overexpress (oe-TLR3) TLR3 in LUSC cell line NCI-H226. The potency of current transfection was confirmed by qRT-PCR and Western blot (Fig. 6A, B). Functional assays demonstrated that TLR3 knockdown significantly reduced cell proliferation (Fig. 6C), migration (Fig. 6D), and colony formation (Fig. 6E), as evidenced by the MTT assay, wound healing assay, and colony formation assay. Conversely, TLR3 overexpression enhanced these processes, indicating its role in promoting LUSC cell growth and migration (Fig. 6C–E). Furthermore, ELISA results showed that TLR3 suppression increased the secretion of pro-inflammatory cytokines TNF-α and IFN-γ, while decreasing IL1β and VEGF levels (Fig. 6F). In contrast, TLR3 overexpression led to elevated levels of IL1β and VEGF, with reduced TNF-α and IFN-γ. All these results indicated that TLR3 played a dual role for cell proliferation and inflammatory response in LUSC.

Discussion

PANoptosis combines characteristics of apoptosis, pyroptosis, and necroptosis, capable of responding to various stress signals through the activation of multiple cell death pathways [30]. Several studies have demonstrated the multifunctional roles of PANoptosis-related genes in LUAD [11], but the exact actions of PANoptosis-related genes in LUSC are still unclear. Therefore, we conducted a comprehensive investigation on the roles of PANoptosis-related genes in LUSC.

In LUSC, 76 PANoptosis-related genes were dysregulated, and these genes were mainly implicated in cell death-related biological processes and immune-inflammatory-related pathways. This was similar with the findings in study of Zhang et al., who found that the dysregulated PANoptosis-related genes in LUAD were principally involved in biological functions of immune function, inflammation and

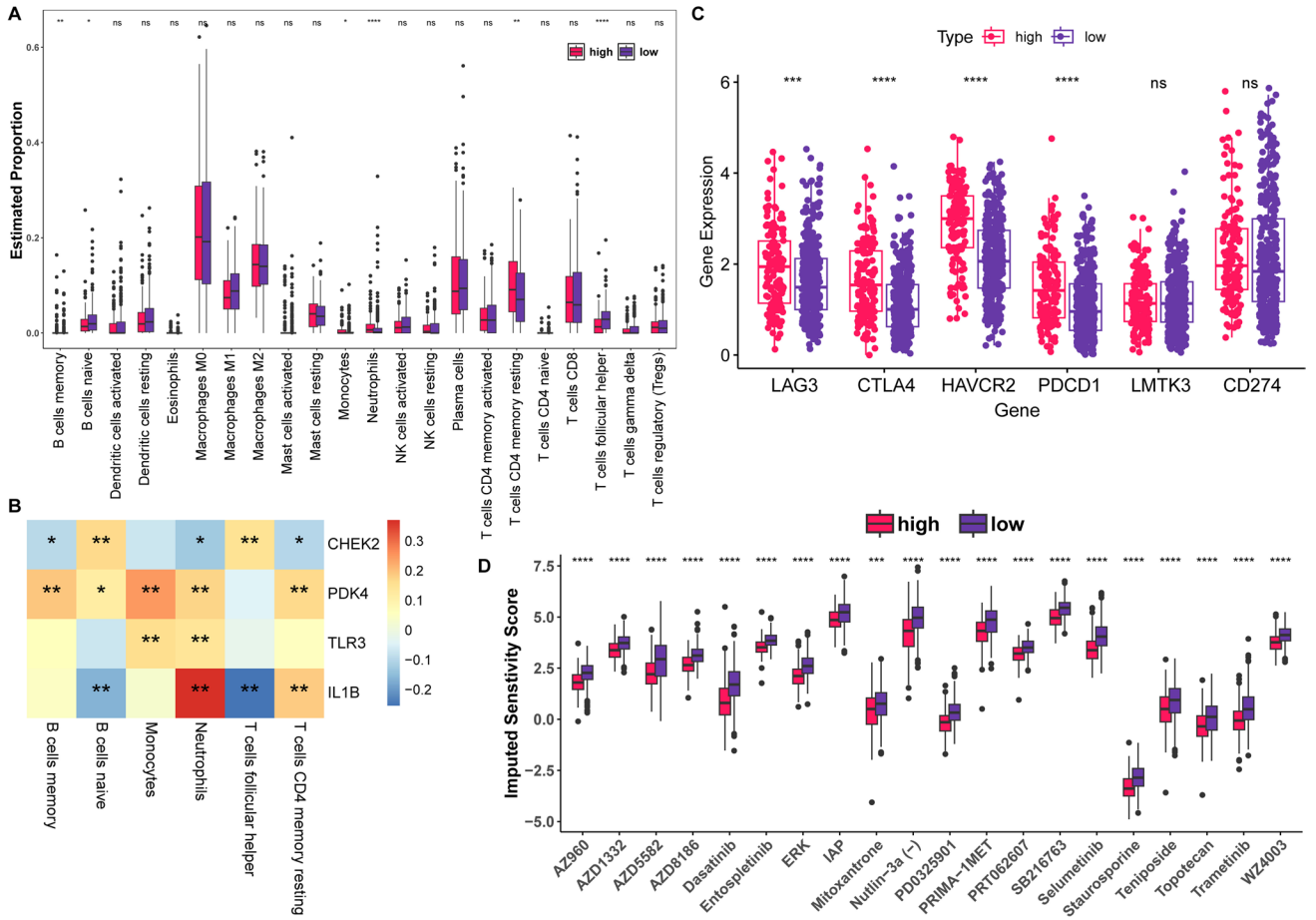

Fig. 4 Immunological analysis and drug sensitive investigation. **A**, box plots showing the differences on infiltrating levels of different immune cells between high-risk group and low-risk group. **B**, the correlation analysis between four prognostic genes and immune cells. **C**, the expression analysis of 6 immune checkpoints between high-risk group and low-risk group. **D**, the drug sensitive analysis between two risk groups. *, $P<0.1$; **, $P<0.05$; ***, $P<0.01$; ****, $P<0.001$

cytokines [11]. Clustering analysis enables the personalized treatment recommendations for individual patients with NSCLC [31] and is also successfully been used to estimate the metastatic patterns from lung cancer [32]. Based on these 76 genes, consensus clustering identified four molecular clusters of LUSC, with cluster 4 showing better survival than the other three. Further investigation of TME revealed that cluster 4 showed the lowest immune score and the highest tumor purity than other clusters. Such phenomenon might be explained by stable genome and high therapy sensitivity (cancer cells with active proliferation are more likely to be killed) of high-purity tumors, while complex TME in low-purity tumors (e.g., fibrotic interstitium) might hinder drug penetration or promote drug resistance [33–35]. Particularly, patients in cluster 2 harbored a high overall immune infiltration level, indicating an immune activation status. This suggested that patients in this cluster might be more likely benefit from immunotherapy. Thus, we speculated that the clustering result in our study might aid in risk stratification of patients, enabling a more accurate prognosis.

Further investigations on prognostic value of these PANoptosis-related DEGs revealed 4 key genes, including CHEK2, PDK4, TLR3, and IL1B. Checkpoint Kinase 2 (CHEK2) is a recognized tumor-inhibiting gene that contribute to the DNA damage response pathway [36]. In lung cancer, CHEK2 has been demonstrated to mediate cell cycle interruption amidst genomic instability, thereby preventing the accumulation of oncogenic mutations [37]. Furthermore, research indicates that the promoted CHEK2 is associated with improved prognosis in patients undergoing radiotherapy [38]. In our study, the upregulation of CHEK2 in LUSC tissues and its inclusion in our prognostic model further supported its role as a key tumor suppressor, potentially helping to counteract oncogenic stress in LUSC. Pyruvate Dehydrogenase Kinase 4 (PDK4) regulates glucose metabolism and is involved in the transition of cells from aerobic glycolysis to oxidative phosphorylation [39]. This

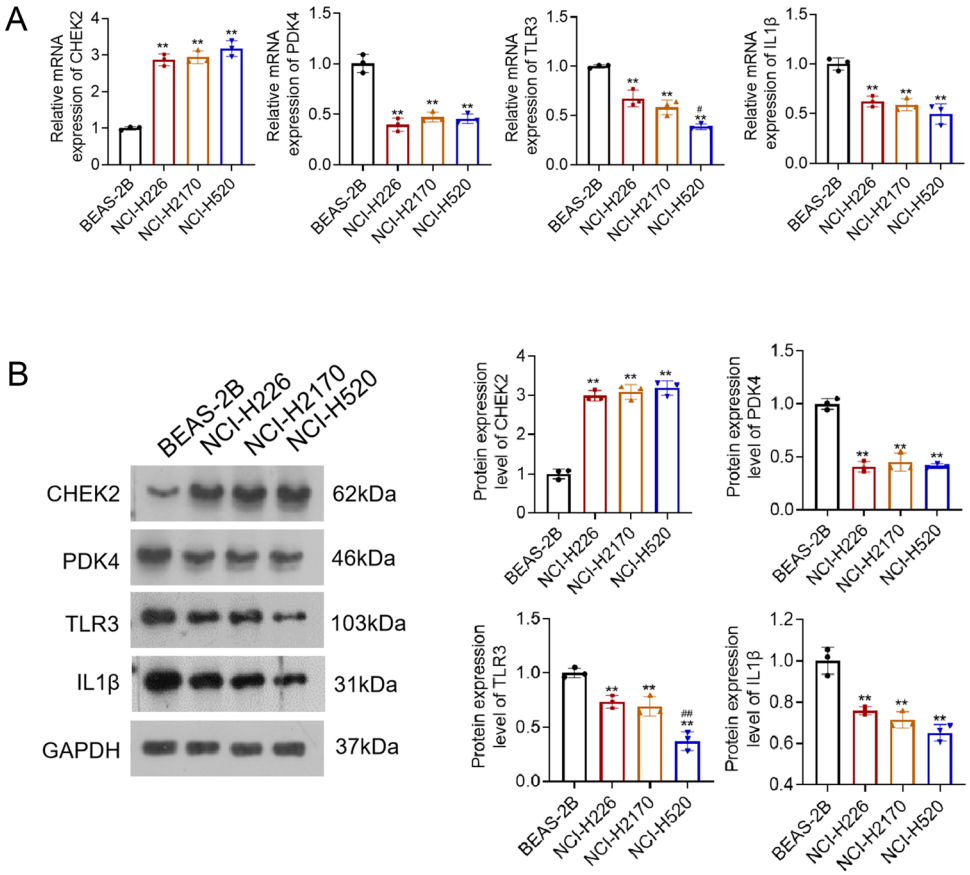

Fig. 5 Expression validation of prognostic genes in human LUSC cells. **A**, the qRT-PCR revealed the expression of each gene in different cell lines at mRNA level. **B**, the Western blot revealed the expression of each gene in different cell lines at protein level. *, $P<0.05$ versus BEAS-2B; **, $P<0.01$ versus BEAS-2B; #, $P<0.05$ versus NCI-H2170; ##, $P<0.01$ versus NCI-H2170

gene has garnered attention for its role in suppressing the Warburg effect, a hallmark of cancer metabolism characterized by the preferential use of glycolysis by tumor cells [40]. Recent studies have indicated that downregulation of PDK4 is associated with aggressive tumor behavior across various cancers, including liver cancers [41]. Specifically, in lung cancer, PDK4 has been found to be reduced in adenocarcinoma, suggesting its tumor-suppressive function [42]. Consistent with these findings, our study showed a significant depression of PDK4 in LUSC tissues, supporting its potential as a therapeutic target to restore normal metabolic processes in cancer cells.

Toll-like receptor 3 (TLR3) is a pattern recognition receptor integral to the system of immune, playing a vital role in detecting viral RNA and activating downstream immune responses [43]. Its role in cancer is complex, as it can promote or suppress tumor development depending on the microenvironment. A previous study has reported that TLR3 activation can induce apoptosis in lung cancer cells, thereby enhancing anti-tumor immunity [44]. However, some studies suggest that dysregulation of TLR3 may lead to tumor escalation by supporting an immunosuppressive niche [44, 45]. In our cytological validation experiments, TLR3 exhibited both pro-tumorigenic and anti-inflammatory effects, indicating that its role in LUSC was context-dependent and might play a dual function in tumor immunity regulation. In addition, the result of our immune analysis showed that TLR3 was closed related to immune cells including neutrophils and monocytes. Neutrophils are the most abundant type of white blood cell, responsible for rapid response and clearance of bacterial infections [46]. In various cancers, especially lung cancer, they exhibit pro-tumor characteristics by promoting an inflammatory microenvironment that supports tumor growth and metastasis [47, 48]. During the recognition of viral RNA and certain pathogens, TLR3 can activate the chemotaxis of neutrophils, promoting their migration to the infection site [49]. This process is facilitated by the release of chemotactic factors and other inflammatory mediators [50]. Monocytes are phagocytes in the immune system that can differentiate into macrophages and dendritic cells to participate in immune responses [51]. Within the tumor microenvironment, they are often induced by the tumor to become pro-tumor macrophages, aiding in immune evasion and tumor cell growth [52]. Under TLR3 activation, monocytes secrete various cytokines, contributing to the inflammatory response process of lung disease [53]. They participate not only in local immune responses but also in systemic inflammation. Since the closed relationship between TLR3 and these two immune cells, we speculated

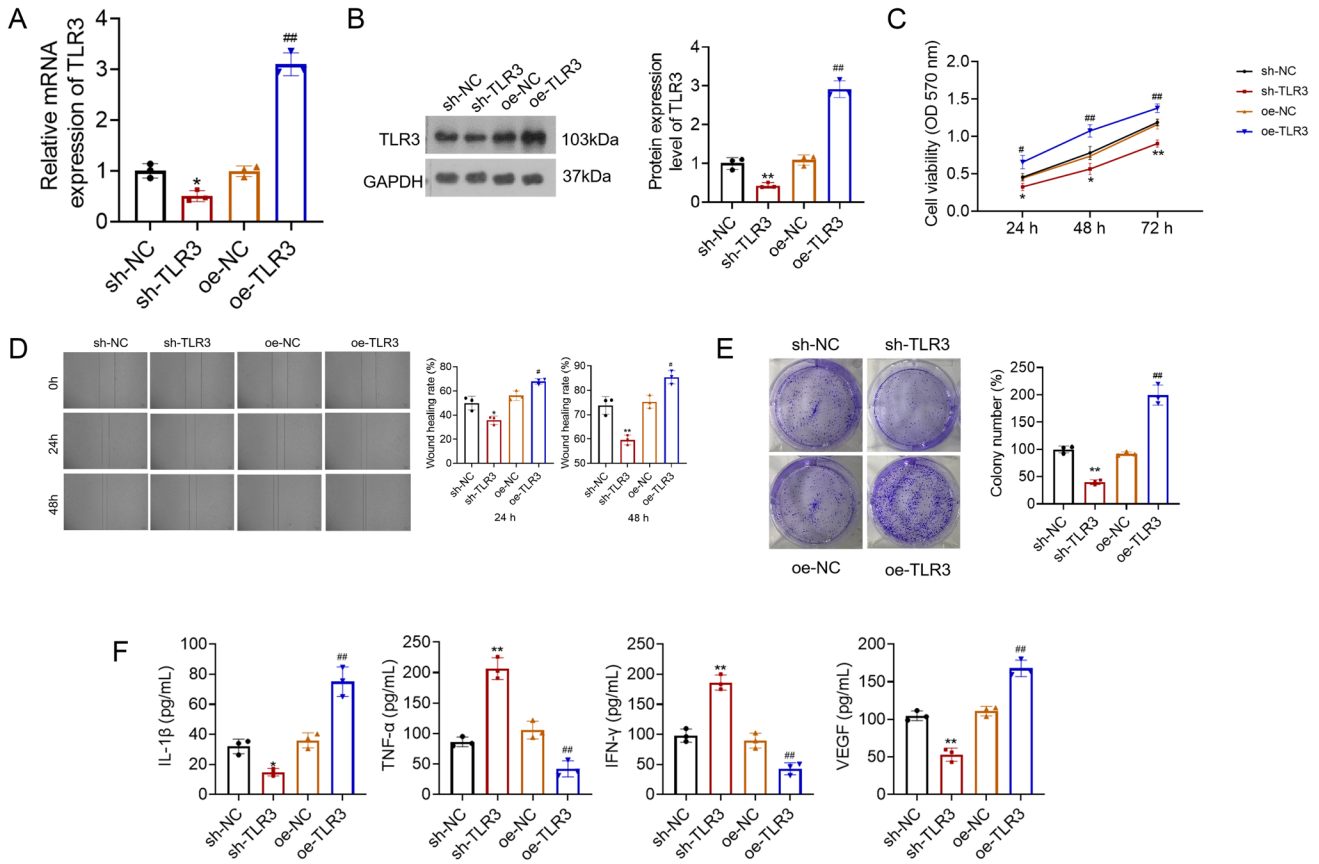

Fig. 6 TLR3 modulated cell proliferation, migration and inflammatory response in LUSC. **A**, the qRT-PCR revealed the expression of TLR3 gene in each treatment group at mRNA level. **B**, the Western blot showed the expression of TLR3 gene in each treatment group at protein level. **C**, MTT assay showed the cell viability in each treatment group. **D**, the wound healing assay showed the cell migration. **E**, the colony formation assay showed the colony formation in each treatment group. **F**, the ELISA assay to detect the expression of immune factors including TNF-α, IFN-γ, VEGF and IL-1β in cell supernatant. *, $P<0.05$ versus sh-NC; **, $P<0.01$ versus sh-NC; #, $P<0.05$ versus oe-NC; ##, $P<0.01$ versus oe-NC

that TLR3 might take part in the progression of LUSC via regulating neutrophils and monocytes.

Interleukin 1-beta (IL1B) is a key cytokine involved in inflammation and immune regulation, with dysregulation linked to various cancers [54]. Elevated levels of IL1B have been demonstrated to facilitate tumor progression by enhancing the inflammatory environment within the tumor microenvironment, promoting angiogenesis, and driving cancer cell proliferation [55, 56]. In lung cancer, IL1B expression is typically decreased in advanced stages, which may contribute to immune evasion [57]. Our study confirmed the downregulation of IL1B in LUSC, reflecting the suppression of inflammatory immune responses within the tumor, further emphasizing its significance as a prognostic biomarker in LUSC. Overall, the prognostic model constructed by using these four genes provided clinicians with a valuable tool for risk stratification of patients and the formulation of tailored therapeutic strategies.

Considering the prognostic value of the identified four genes, a risk model was then established, which predicted the prognosis of LUSC patients with moderate accuracy. The risk model could facilitate risk stratification of LUSC patients. Patients in high-risk group had a high expression of immune checkpoints, such as PD-1 and CTLA4, indicating that these patients might be more likely benefit from ICB therapy. These findings are helpful to develop a relatively personalized treatment plan in clinical. Moreover, these four genes constructed risk model contributed to reflect the drugs sensitivity. High-risk patients exhibited increased sensitivity to certain anti-tumor agents, such as AZD8186 and Topotecan. AZD8186 is a PI3K inhibitor that can affect cell proliferation and survival. By inhibiting the PI3K/AKT pathway, it may trigger cell death and increase the sensitivity of tumor cells to chemotherapy agents [58]. Topotecan, a topoisomerase inhibitor, primarily induces apoptosis by interfering with DNA replication and transcription [59]. While it is commonly used for small cell lung cancer, it has

shown efficacy in certain cases of squamous lung cancer as well [60]. This result suggested that targeting PANoptosis-related pathways might enhance therapeutic efficacy, particularly in overcoming resistance to conventional therapies. Clinically, our findings support the incorporation of PANoptosis-based strategies to improve the efficacy of current treatments for LUSC. For instance, therapies that promote PANoptosis could enhance the immune response against tumors, reduce tumor burden, and improve patient survival outcomes [17]. These results not only lay the groundwork for further investigation into the mechanisms of PANoptosis in tumors but also provide a novel view for anti-tumor therapeutic strategies.

Although this study fills a gap in the study of PANoptosis-related genes in LUSC, we must admit that this is a preliminary exploratory study with several limitations. First, the key genes and their prognostic values were investigated mainly depend on the data from public databases, and hence, prospective cohort studies with large sample size in the real world are essential to test the prognostic value of key genes, the predictive power of the risk model, as well as the correlations of with treatment responses. Second, expression of key genes was confirmed only in cell lines, but not in clinical tumor tissue samples. Besides, the exact roles of other three genes in addition to TLR3 have not been investigated. These are the directions of our next studies. Even more, the drugs that may target these genes should be further explored to further discover the exact roles of these genes in the progression of LUSC.

In conclusion, this study identified four PANoptosis-related molecular subtypes in LUSC with diverse survival and TME and also highlighted the potential of CHEK2, PDK4, TLR3, and IL1B as biomarkers or targets in LUSC. The risk model established by these four genes contributed to risk stratification, prognosis and treatment response prediction for patients with LUSC, which provided novel insights to develop personalized treatment strategy for patients with LUSC.

Supplementary Information The online version contains supplementary material available at https://doi.org/10.1007/s10238-025-01696-x.

Acknowledgements Not applicable.

Author contributions Conceptualization was done by Ying Chen and Meihua Wang; data curation, formal analysis, investigation and methodology were done by Ying Chen and Meihua Wang; project administration, resources and supervision were done by Meihua Wang; software was done by Ying Chen; validation was done by Meihua Wang; visualization and writing—original draft were done by Ying Chen; writing—review and editing was done by Ying Chen and Meihua Wang. All authors reviewed the results and approved the final version of the manuscript.

Funding The Zhejiang Province Medical and Health Science and Technology Plan [Grant Number 2022KY1026].

Data availability No datasets were generated or analyzed during the current study.

Declarations

Conflict of interest The authors declare no competing interests.

Statement of ethics This article does not involve any animal or human experimentation.

References

1. Lau SCM, et al. Squamous cell lung cancer: Current landscape and future therapeutic options. Cancer Cell. 2022;40(11):1279–93.
2. Scagliotti G, et al. The differential efficacy of pemetrexed according to NSCLC histology: a review of two Phase III studies. Oncologist. 2009;14(3):253–63.
3. Zinner RG, et al. Comparison of patient outcomes according to histology among pemetrexed-treated patients with stage IIIB/IV non-small-cell lung cancer in two phase II trials. Clin Lung Cancer. 2010;11(2):126–31.
4. Kujtan L, et al. Squamous cell carcinoma of the lung: improving the detection and management of immune-related adverse events. Expert Rev Anticancer Ther. 2022;22(2):203–13.
5. Wang M, Herbst RS, Boshoff C. Toward personalized treatment approaches for non-small-cell lung cancer. Nat Med. 2021;27(8):1345–56.
6. Adib E, et al. Variation in targetable genomic alterations in non-small cell lung cancer by genetic ancestry, sex, smoking history, and histology. Genome Med. 2022;14(1):39.
7. Sun X, et al. PANoptosis: mechanisms, biology, and role in disease. Immunol Rev. 2024;321(1):246–62.
8. Zhu P, et al. Advances in mechanism and regulation of PANoptosis: prospects in disease treatment. Front Immunol. 2023;14:1120034.
9. Pandian N, Kanneganti TD. PANoptosis: a unique innate immune inflammatory cell death modality. J Immunol. 2022;209(9):1625–33.
10. Yang Y, et al. Identification and cross-validation of autophagy-related genes in cardioembolic stroke. Front Neurol. 2023;14:1097623.
11. Zhang C, et al. Identifying prognostic genes related PANoptosis in lung adenocarcinoma and developing prediction model based on bioinformatics analysis. Sci Rep. 2023;13(1):17956.

12. Miao Z, Yu W. Significance of novel PANoptosis genes to predict prognosis and therapy effect in the lung adenocarcinoma. Sci Rep. 2024;14(1):20934.
13. Zhao X, et al. Exploration of the prognostic prediction value of the PANoptosis-based risk score and its correlation with tumor immunity in lung adenocarcinoma. J Gene Med. 2024;26(3): e3682.
14. Zhou X, et al. Identification of PANoptosis subtypes to assess the prognosis and immune microenvironment of lung adenocarcinoma patients: a bioinformatics combined machine learning study. Curr Cancer Drug Targets, 2024.
15. Goldman MJ, et al. Visualizing and interpreting cancer genomics data via the Xena platform. Nat Biotechnol. 2020;38(6):675–8.
16. Edgar R, Domrachev M, Lash AE. Gene expression omnibus: NCBI gene expression and hybridization array data repository. Nucleic Acids Res. 2002;30(1):207–10.
17. Song F, et al. PANoptosis-based molecular subtyping and HPAN-index predicts therapeutic response and survival in hepatocellular carcinoma. Front Immunol. 2023;14:1197152.
18. Love MI, Huber W, Anders S. Moderated estimation of fold change and dispersion for RNA-seq data with DESeq2. Genome Biol. 2014;15(12):550.
19. Rosell-Díaz M, et al. Metformin-induced changes in the gut microbiome and plasma metabolome are associated with cognition in men. Metabolism. 2024;157: 155941.
20. Szklarczyk D, et al. The STRING database in 2017: quality-controlled protein–protein association networks, made broadly accessible. Nucleic acids research, 2016: p. gkw937.
21. Wu T, et al. clusterProfiler 4.0: a universal enrichment tool for interpreting omics data. Innovation (Camb). 2021;2(3):100141.
22. Wilkerson MD, Hayes DN. ConsensusClusterPlus: a class discovery tool with confidence assessments and item tracking. Bioinformatics. 2010;26(12):1572–3.
23. Yoshihara K, et al. Inferring tumour purity and stromal and immune cell admixture from expression data. Nat Commun. 2013;4:2612.
24. Tibshirani R. The lasso method for variable selection in the Cox model. Stat Med. 1997;16(4):385–95.
25. Chen B, et al. Profiling tumor infiltrating immune cells with CIBERSORT. Methods Mol Biol. 2018;1711:243–59.
26. Hu D, Zhou M, Zhu X. Deciphering immune-associated genes to predict survival in clear cell renal cell cancer. Biomed Res Int. 2019;2019:2506843.
27. Bachner J, et al. Multi-level validation of the German physical activity self-efficacy scale in a sample of female sixth-graders. BMC Public Health. 2020;20(1):1–10.
28. Maeser D, Gruener RF, Huang RS. oncoPredict: an R package for predicting in vivo or cancer patient drug response and biomarkers from cell line screening data. Brief Bioinform. 2021. https://doi.org/10.1093/bib/bbab260.
29. Livak KJ, Schmittgen T. Analysis of relative gene expression data using real-time quantitative PCR and the 2−ΔΔCT method. Methods. 2001;25(4):402–8. https://doi.org/10.1006/meth.2001.1262.
30. Wang Y, Kanneganti TD. From pyroptosis, apoptosis and necroptosis to PANoptosis: a mechanistic compendium of programmed cell death pathways. Comput Struct Biotechnol J. 2021;19:4641–57.
31. Shen Y, et al. Pharmacogenomic cluster analysis of lung cancer cell lines provides insights into preclinical model selection in NSCLC. Interdiscip Sci. 2022;14(3):712–21.
32. Watanabe H, et al. Application of cluster analysis to distant metastases from lung cancer. Anticancer Res. 2020;40(1):413–9.
33. Wang S, et al. Prognostic value of four immune-related genes in lower-grade gliomas: a biomarker discovery study. Front Genet. 2024;15:1403587.
34. Zhao F, et al. Exploring the potential of exosome-related LncRNA pairs as predictors for immune microenvironment, survival outcome, and microbiotain landscape in esophageal squamous cell carcinoma. Front Immunol. 2022;13: 918154.
35. Han Y, et al. Development and validation of prognostic index based on immunogenic cell death-related genes with melanoma. Front Oncol. 2022;12:1011046.
36. Stolarova L, et al. CHEK2 germline variants in cancer predisposition: stalemate rather than checkmate. Cells. 2020;9(12):2675. https://doi.org/10.3390/cells9122675.
37. Chang YS, et al. Mutation profile of non-small cell lung cancer revealed by next generation sequencing. Respir Res. 2021;22(1):3.
38. Morra A, et al. Association of the CHEK2 c.1100delC variant, radiotherapy, and systemic treatment with contralateral breast cancer risk and breast cancer-specific survival. Cancer Med. 2023;12(15):16142–62.
39. Dou X, et al. PDK4-dependent hypercatabolism and lactate production of senescent cells promotes cancer malignancy. Nat Metab. 2023;5(11):1887–910.
40. Weng Y, et al. The miR-15b-5p/PDK4 axis regulates osteosarcoma proliferation through modulation of the Warburg effect. Biochem Biophys Res Commun. 2018;503(4):2749–57.
41. Si T, et al. Ruangan Lidan decoction inhibits the growth and metastasis of liver cancer by downregulating miR-9-5p and upregulating PDK4. Cancer Biol Ther. 2023;24(1):2246198.
42. Yu S, et al. PDK4 promotes tumorigenesis and cisplatin resistance in lung adenocarcinoma via transcriptional regulation of EPAS1. Cancer Chemother Pharmacol. 2021;87(2):207–15.
43. Zheng Y, et al. Glioma-derived ANXA1 suppresses the immune response to TLR3 ligands by promoting an anti-inflammatory tumor microenvironment. Cell Mol Immunol. 2024;21(1):47–59.
44. Bianchi F, et al. TLR3 expression induces apoptosis in human non-small-cell lung cancer. Int J Mol Sci. 2020;21(4):1440. https://doi.org/10.3390/ijms21041440.
45. Tolstova T, et al. The effect of TLR3 priming conditions on MSC immunosuppressive properties. Stem Cell Res Ther. 2023;14(1):344.
46. Chan L, et al. The roles of neutrophils in cytokine storms. Viruses. 2021;13(11):2318. https://doi.org/10.3390/v13112318.
47. Salcher S, et al. High-resolution single-cell atlas reveals diversity and plasticity of tissue-resident neutrophils in non-small cell lung cancer. Cancer Cell. 2022;40(12):1503-1520.e8.
48. Xiao Y, et al. Cathepsin C promotes breast cancer lung metastasis by modulating neutrophil infiltration and neutrophil extracellular trap formation. Cancer Cell. 2021;39(3):423-437.e7.
49. Liu Y, et al. Tumor exosomal RNAs promote lung Pre-metastatic niche formation by activating alveolar epithelial TLR3 to recruit neutrophils. Cancer Cell. 2016;30(2):243–56.
50. Muendlein HI, et al. Neutrophils and macrophages drive TNF-induced lethality via TRIF/CD14-mediated responses. Sci Immunol. 2022. https://doi.org/10.1126/sciimmunol.add0665.
51. Ganesh RN, Garcia G, Truong L. Monocytes and macrophages in kidney disease and homeostasis. Int J Mol Sci. 2024;25(7):3763. https://doi.org/10.3390/ijms25073763.
52. Watanabe R, Hashimoto M. Pathogenic role of monocytes/macrophages in large vessel vasculitis. Front Immunol. 2022;13: 859502.
53. Wang X, et al. TLR3-activated monocyte-derived dendritic cells trigger progression from acute viral infection to chronic disease in the lung. J Immunol. 2021;206(6):1297–314.
54. Karpenko D, et al. Functional characteristics of the mouse Il1b promoter in various tissues before and after irradiation. DNA Cell Biol. 2020;39(5):790–800.

55. Zhu J, Guo Y. Circ_0020093 Overexpression Alleviates Interleukin-1 Beta-induced Inflammation, apoptosis and extracellular matrix degradation in human chondrocytes by targeting the miR-181a-5p/ERG pathway. Immunol Invest. 2022;51(6):1660–77.
56. Zhang J, et al. Exogenous interleukin-1 beta promotes the proliferation and migration of HeLa cells via the MEK/ERK signaling pathway. Mol Biol Rep. 2022;49(5):3765–72.
57. Yin J, et al. Common variants of pro-inflammatory gene IL1B and interactions with PPP1R13L and POLR1G in relation to lung cancer among Northeast Chinese. Sci Rep. 2023;13(1):7352.
58. Asati V, et al. Recent advances in PI3 kinase inhibitors: anticancer activities and structure-activity relationships. Mini Rev Med Chem. 2022;22(16):2146–65.
59. Lambrecht L, et al. Topotecan in a real-world small-cell lung cancer cohort: prognostic biomarkers improve selection of patients for second-line treatment. Diagnostics. 2024;14(14):1572. https://doi.org/10.3390/diagnostics14141572.
60. Edelman MJ, et al. Randomized phase 3 study of the anti-disialoganglioside antibody dinutuximab and irinotecan vs irinotecan or topotecan for second-line treatment of small cell lung cancer. Lung Cancer. 2022;166:135–42.